Shape-Dependent Electronic Excitations in Metallic Chains

Bin Gao,*,† Kenneth Ruud,† and Yi Luo‡,¶

Centre for Theoretical and Computational Chemistry (CTCC), Department of Chemistry, University of Tromsø—The Arctic University of Norway, N–9037 Tromsø, Norway, Department of Theoretical Chemistry, School of Biotechnology, Royal Institute of Technology, SE–10691 Stockholm, Sweden, and Hefei National Laboratory for Physical Sciences at the Microscale, University of Science and Technology of China, Hefei, Anhui 230026, P. R. China

E-mail: bin.gao@uit.no

*To whom correspondence should be addressed

†Centre for Theoretical and Computational Chemistry (CTCC), Department of Chemistry, University of Tromsø—The Arctic University of Norway, N–9037 Tromsø, Norway

‡Department of Theoretical Chemistry, School of Biotechnology, Royal Institute of Technology, SE–10691 Stockholm, Sweden

¶Hefei National Laboratory for Physical Sciences at the Microscale, University of Science and Technology of China, Hefei, Anhui 230026, P. R. China

Abstract

The electronic excitations of silver chains with different geometries (linear, circle, arc and zigzag chains) have been investigated at the time-dependent density functional theory level, by solving the equation of motion of the reduced single-electron density matrix in the real-time domain. A scaling parameter $0 \leq \lambda \leq 1$ has been introduced to adjust the two-electron contributions during propagation in the time domain in a way that allows us to distinguish different electronic excitations — plasmon and single-particle excitations. The dipole responses, in particular the plasmon resonances of these metallic chains to an external δ-pulse, show a strong dependence on their geometric structures. In most cases, the dipole responses of these chains possess great tunability when altering their geometric parameters — the radius of the circle and arc chains, and the bond angle of the zigzag chains. Some excitations in these chains also show a wide tunable excitation energy range, more than 1 eV, making it possible to fine-tune the excitations of the metallic chains at an atomic scale.

Keywords: metallic chains, electronic excitations, plasmon, time-dependent density functional theory

1 INTRODUCTION

Compared to higher-dimensional systems, quasi-one-dimensional metallic chains are believed to possess unique properties because the electrons can move rather freely in the one dimension defined by the arrangement of the atoms but finite and very limited extension in the other two dimensions.[1] Due to their simple geometric structures and the unique behaviour of the electronic motions, metallic chains have been extensively investigated in recent years — their formation,[2–4] geometries,[1,5–7] stabilities,[1,8–10] electronic structures,[1,5,6,8–10] conductivity[11] and spectroscopic properties[12–15] have all been studied. Especially, the plasmons (collective oscillations of the conduction electrons)[16] in these artificial metallic chains have also

received particular attention. Yan *et al.* studied the electronic excitations of sodium, potassium and silver linear chains at the time-dependent density functional theory (TDDFT) level.[12,13] Similar study of the dipole responses of gold chains Au_{2n} ($n = 1, 2, \cdots, 10$) was reported by Lian *et al.*[14] at the TDDFT level in the frequency domain using the linear response method, but limited to a finite energy range. We recently implemented the real-time TDDFT method in a tool package TDRSP,[17] in which the reduced single-electron density matrix is propagated according to the Liouville-von Neumann equation after an impulse excitation. The corresponding dipole responses in the frequency domain (optical absorption) can be retrieved using a subsequent Fourier transformation. The use of time propagation allows us to access a wide frequency range and in particular to access states of high energy, difficult to reach using conventional response theory in the frequency domain. By utilizing this method, we have successfully investigated the electronic excitations of three noble-metal chains — copper, silver and gold — with up to 26 atoms at the TDDFT level.[18]

In a recent work, Bernadotte *et al.* proposed a scaling approach analysis[19] to distinguish plasmons and single-particle excitations in molecules, in which a scaling parameter $0 \leq \lambda \leq 1$ was introduced in order to adjust the two-electron contributions in the TDDFT eigenvalue equations. By tracking the dependence of individual excitations on the λ parameter, they successfully discriminated plasmon and single-particle excitations in different systems such as metal chains and clusters.[19,20] In a study of electronic excitations in different gold nanowires, Piccini *et al.*[21] employed this idea of a scaling approach analysis to discriminate different electronic excitations. We will here use the scaling approach analysis in real-time TDDFT, allowing us to reveal different excitations, in particular the plasmons in different metallic chains, from the real-time TDDFT calculation.

The study of plasmons in metallic chains can rationalize the occurence surface plasmons appearing in higher-dimensional systems. For instance, various surface-enhanced spectroscopies[16] have become active research areas both experimentally and theoretically, because understanding the interaction of plasmon resonances on the metallic surface with

atoms/molecules adsorbed on the surface is needed in order to understand the mechanisms that govern these surface-enhanced spectroscopies. Moreover, in order to utilize the full potential of metallic nanomaterials in different applications, their plasmons must be tunable, for instance at nanometre scale or subnanometre scale.[12] In the aforementioned studies, different electronic excitations have been observed in the metallic chains and shown to be tunable by changing the chain length. Yan *et al.* also demonstrated the possibility of controlling the plasmons in a sodium chain by attaching a silver atom at one end of the chain.[12]

Another important factor that affects the excitations of nanomaterials is their geometric structures.[16,22] Although different geometries of the metallic chains, for example, linear, zigzag, helix and tetragonal chains, have been investigated theoretically in terms of their structure, stability and electronic properties,[1,5–7] a detailed study of the dipole responses of these different metallic chains still needs to be explored, in particular at the level of TDDFT.

The purpose of this paper is therefore to provide a detailed and comparative study of the electronic excitations in the metallic chains with different geometries: circle, arc and zigzag. We will take the silver chains as an example to demonstrate the shape-dependent electronic excitations in the metallic chains. We will use the real-time TDDFT method as implemented in our tool package TDRsp.[17] This allows us to obtain a deep understanding of the different electronic excitations in various metallic chains, of interest both for theoretical and experimental studies, including different surface-enhanced spectroscopies.

The remainder of this paper is organized as follows: the computational details are described in Section 2, followed by results and discussion in Section 3. Our concluding remarks are given in Section 4.

2 COMPUTATIONAL DETAILS

In this work, we will consider silver chains with three different geometries as shown in Fig. 1: circle, arc and zigzag. To exclude other factors that could affect the electronic excitations,

we have fixed the internuclear distance between the silver atoms at the experimental value of 2.89 Å[23] in all the different silver chains. As such, the number of atoms in the chains, the radius R of the circle and arc chains (or their curvature $1/R$), and the bond angle θ of the zigzag chains become the key structural factors affecting the electronic excitations of these chains.

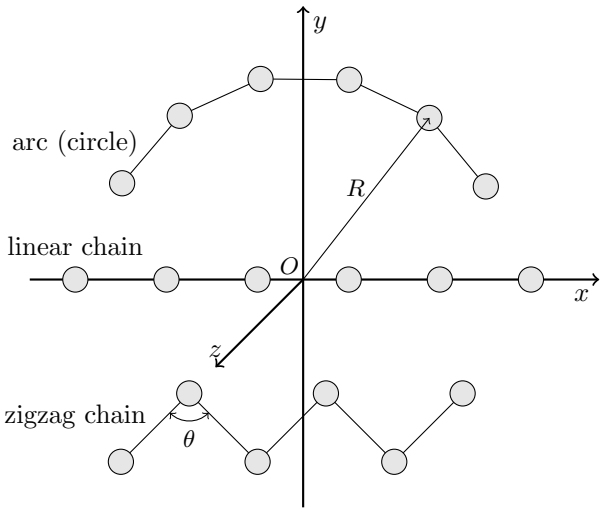

Figure 1: Schematic drawing of metallic chains with different structures studied in current work.

As in our previous study on plasmon resonances in linear noble-metal chains,[18] we have chosen to propagate the reduced single-electron density matrix $\mathbf{D}(t)$ according to the Liouville-von Neumann equation in the real-time domain[18]

$$\mathrm{i}\frac{\partial \mathbf{D}(t)}{\partial t} = [\mathbf{F}(t) + \mathbf{V}(t)]\,\mathbf{D}(t) - \mathbf{D}(t)\,[\mathbf{F}(t) + \mathbf{V}(t)]\,, \tag{1}$$

using orthogonal basis sets. Here $\mathbf{F}(t)$ is the Fock matrix defined as

$$\mathbf{F}(t) = \mathbf{h} + \mathbf{G}(\mathbf{D}(t)), \tag{2}$$

with $\mathbf{h}$ the one-electron Hamiltonian and with $\mathbf{G}$ contains different two-electron contributions such as Coulomb and exchange-correlation contributions.

The matrix $\mathbf{V}(t)$ represents the external perturbations as

$$\mathbf{V}(t) = \sum_A \varepsilon_A(t)\mathbf{A}, \tag{3}$$

with $\mathbf{A}$ being the dipole moments along, for instance, the x, y and z directions as defined in Fig. 1. For the case of a δ-pulse as studied here, $\varepsilon_A(t) = \varepsilon\delta(t)$.

To further discriminate between single-particle and plasmon excitations, we employ the scaling approach analysis of Bernadotte *et al.*[19,20] rewriting the Fock matrix as

$$\mathbf{F}_\lambda(t) = \mathbf{h} + (1-\lambda)\mathbf{G}(\mathbf{D}_0) + \lambda\mathbf{G}(\mathbf{D}(t)),\ 0 \leq \lambda \leq 1, \tag{4}$$

where $\mathbf{D}_0$ is the density matrix of the ground state determined from the self-consistent field calculation (i.e., before the δ-pulse is applied) and thus $\mathbf{G}(\mathbf{D}_0)$ represents the ground-state two-electron contributions. The parameter λ is introduced to scale the two-electron contributions $\mathbf{G}(\mathbf{D}(t))$ during the time propagation. Obviously, $\mathbf{F}_\lambda(t) = \mathbf{F}(t)$ in Eq. (2) for $\lambda = 1$, and $\mathbf{F}_\lambda(t) = \mathbf{h} + \mathbf{G}(\mathbf{D}_0) = \mathbf{F}(0)$ for $\lambda = 0$ as two extreme cases of the parametrization in Eq. (4). In the latter case, the Fock matrix is during the propagation fully represented by that of the ground state, and the electron–electron interactions after the δ-pulse have been applied are completely suppressed. By adjusting the λ parameter, different types of electronic excitations can be distinguished:[19,20] those whose excitation energies are sensitive to the scaling factor λ may belong to plasmonic excitations, whereas the others can be classified as single-particle excitations whose excitation energies show slight dependence on the parameter λ.

These different electronic excitations can be obtained from the absorption spectrum, which is described by the dipole strength function $S(\omega)$ at frequency ω[24]

$$S(\omega) = \frac{4\pi\alpha_{\text{fs}}\omega}{3\varepsilon}\text{Tr}\left[\text{Im}\boldsymbol{\alpha}(\omega)\right], \tag{5}$$

where α_{fs} is the fine-structure constant, ε is the strength of the external δ-pulse (which is chosen as 0.05 eV/bohr in this study), and $\boldsymbol{\alpha}(\omega)$ the complex polarizability tensor obtained from the Fourier transformation of its time-dependent counterpart $\boldsymbol{\alpha}(t)$.

The time-dependent polarizability tensor $\boldsymbol{\alpha}(t)$ can be calculated from $\mathbf{D}(t)$, which is obtained by the fourth-order Runge-Kutta method with a time step of 0.02 a.u. and a total propagation time of 1500 a.u. The propagation of the density matrix $\mathbf{D}(t)$ has been performed by the TDRSP library,[17] in which the two-electron contributions $\mathbf{G}(\mathbf{D}(t))$ of the Fock matrix are calculated through callback functions to a local version of the DALTON program.[25]

All calculations in this work have been performed at the TDDFT level using the Perdew-Wang 91 exchange–correlation functional.[26] The pseudopotential of the Stuttgart/Cologne group ECP28MWB (derived at the quasi-relativistic level) has been employed, together with the corresponding effective core potential basis set $(7s7p5d)/[5s5p2d]$.[27]

3 RESULTS AND DISCUSSION

3.1 Circle Chains

The dipole responses of circle chains Ag_{2n} $(n = 5, 6, \cdots, 11)$ and two linear chains Ag_{12} and Ag_{22} (two topmost) are shown in Fig. 2(a) and (b), in which the radii of the circle chains are also given in the parentheses. As observed also in the case of linear metallic chains,[18] the dipole responses of the circle chains can be divided in two different classes corresponding to the external δ-pulse polarized (a) parallel with the circle chains (named as parallel mode hereafter) and (b) perpendicular to the chains (named as transverse mode hereafter), respectively.

As seen from Fig. 2(a) and (b), there are similarities between the dipole responses of the linear and circle chains:

1. As is the case for the first peak of the linear chains in the longitudinal mode, the first

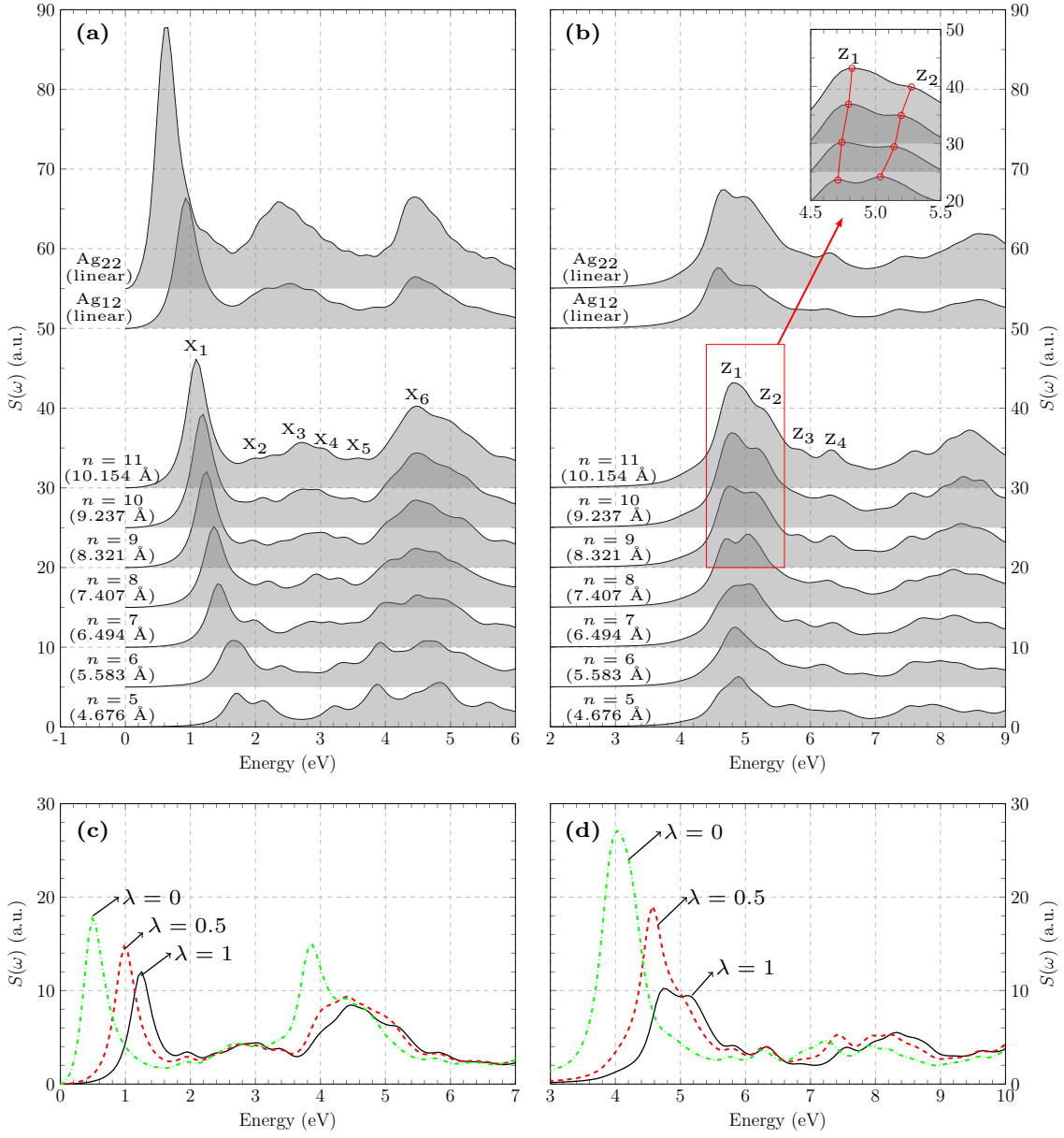

Figure 2: Top: the dipole responses of Ag_{2n} ($n = 5, 6, \cdots, 11$) circle chains and two linear chains Ag_{12} and Ag_{22} (topmost) to an external δ-pulse with strength 0.05 eV/bohr and polarized along (a) x and (b) z directions. Bottom: the dipole responses of the Ag_{18} circle chain to the same external δ-pulse polarized along (c) x and (d) z directions with different scaling parameter λ.

peak X_1 of the circle chains is red-shifted with the increasing chain radius as shown in Fig. 2(a), and its intensity increases when the circle chain becomes larger;

2. The peak X_6 splits for circle chains with smaller radii (Ag_{10} and Ag_{12}), and stays almost fixed at 4.46 eV for chains with larger radii, being very similar to the corresponding excitation energy in the case of longer linear chains, 4.44 eV.[18] For shorter linear chains, such as Ag_2, Ag_4 and Ag_6, the split of this peak was also observed in our previous study;[18] As will be discussed below, this peak may involve a mixing of plasmon and single-particle excitations, and the disappearance of the split of this peak could be due to the much more excitations involved in the larger circle and longer linear chains;

3. For circle chains with larger radii (Ag_{16}–Ag_{22}), the energy of the first two peaks Z_1 and Z_2 in the transverse mode are slightly blue-shifted with increasing chain radius (as shown in the inset of Fig. 2(b)), as also observed in the case of linear chains for increasing chain lengths.[18]

However, there are also obvious differences between the dipole responses of the circle and linear chains, in particular in the longitudinal mode. Using the Ag_{22} chains as an example, the energy of the X_1 peak in the circle chain is slightly larger than that of the linear chain, whereas the intensity of this peak is much higher in the linear chain as can be seen from Fig. 2(a). We also notice that peaks X_2–X_5 in the circle chain are less intense than those in the linear chain.

In Fig. 2(c) and (d), we also present the dipole responses of the Ag_{18} circle chain to the same external δ-pulse but with different scaling parameters λ (see Eq. (4)). Peaks X_1, X_6, Z_1 and Z_2 are sensitive to the scaling parameter λ and are blue-shifted with increasing λ values. Within the random-phase approximation, Bernadotte *et al.* have got the following plasmon dispersion of a noninteracting homogeneous electron gas model[19]

$$\omega_{\rm plas}^2(q) = \frac{4\pi e^2 \rho_0}{m}\lambda + \nu_{\rm F}^2 q^2, \tag{6}$$

where e, ρ_0 and m are respectively the electron charge, the electron density and the (effective) electron mass. ν_{F} and q are the Fermi velocity and the wavevector of the excitation. This plasmon dispersion clearly demonstrates the blue shift of plasmons with the increasing λ values. For the real complicated system and the TDDFT calculations, although the plasmon dispersion is different from this simple model, the blue shift behavior of the plasmon is also expected.[19]

Piccini *et al.*[21] further demonstrated that a characteristic of plasmon resonances is the mixing of many configurations' transitions. In the top panel of Fig. 3, the fluctuations of the occupation numbers of different molecular orbitals (MOs) in the Ag_{18} circle chain are shown for these four peaks, calculated from the equation[18,28]

$$\Delta n^{\mu}(\omega) = \mathrm{diag}\left[\mathbf{C}_0^{\dagger}\mathbf{P}^{\mu}\left(\mathbf{D}(\omega) - \mathbf{D}_0\right)\mathbf{C}_0\right], \tag{7}$$

with $\mathbf{C}_0$ being the MO coefficients before the δ-pulse is added, and $\mathbf{P}^{\mu}$ the operator projecting the density matrix onto some atomic orbitals ξ_{μ}.

From the fluctuations of the occupation numbers of the different MOs (red open bars) in Fig. 3, we see that more than one MO transition is involved in peaks X_1, X_6, Z_1 and Z_2 in the Ag_{18} circle chain, in particular in the case of the peaks Z_1 and Z_2. As such, except for the peak X_6 (which may involve a mixing of plasmon and single-particle excitations, see the discussion of Fig. 5 in Section 3.2), others can safely be assigned as plasmon resonances. Moreover, by projecting the density matrix onto the atomic d orbitals, as shown in the blue bars in Fig. 3, we find that the X_6 peak is the first one in the parallel mode that involves d electron, in agreement with our observation for linear chains.[18] In the transverse mode, there are in most cases $d \rightarrow p$ transitions in each resonance, as also observed in the linear chains.[18]

In the lower panel of Fig. 3, we have also plotted the induced electron densities of the peaks X_1, X_6, Z_1 and Z_2 in the Ag_{18} circle chain as well as those of the corresponding peaks

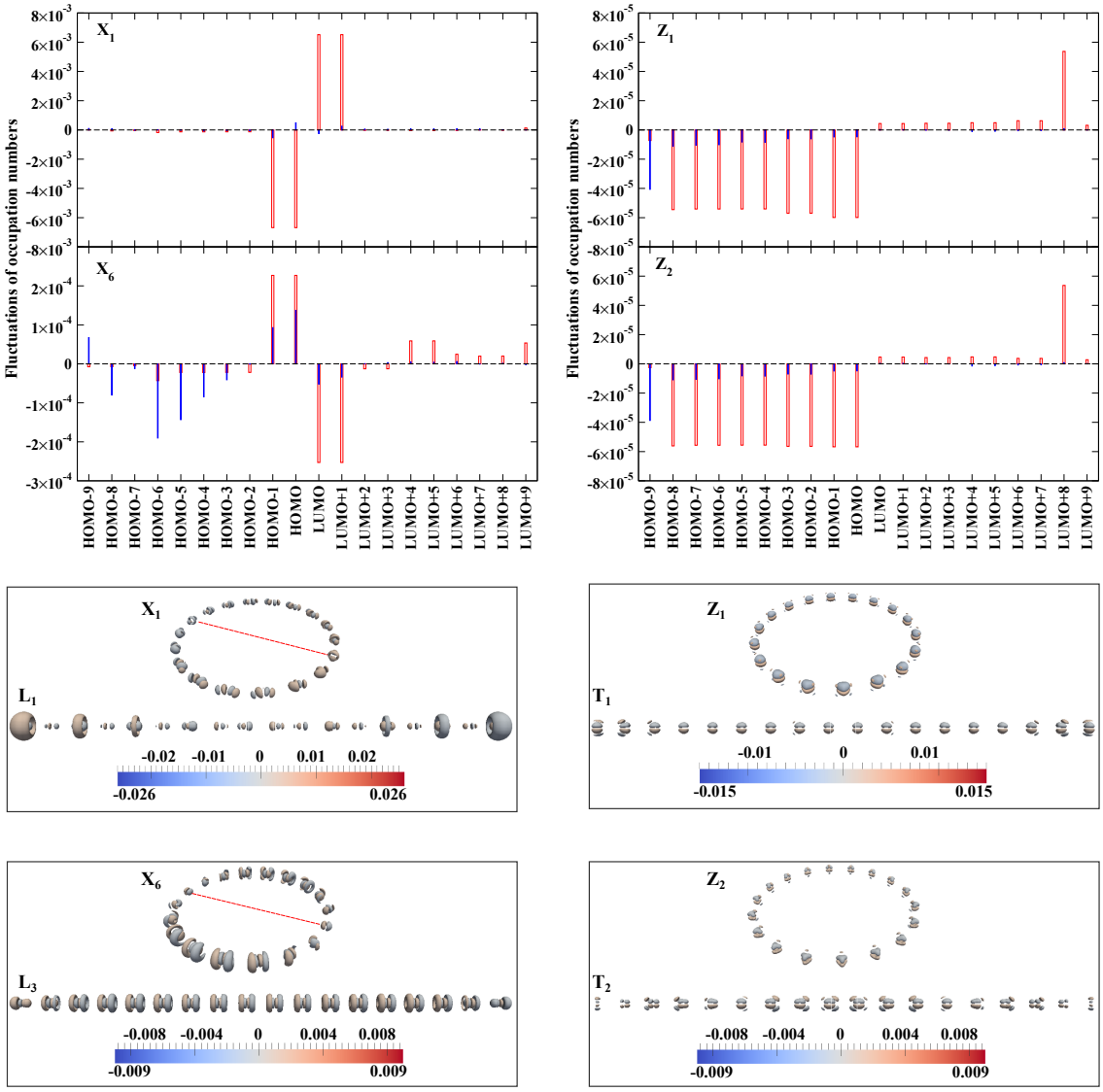

Figure 3: Top: fluctuations of occupation numbers of MOs (red open bars) and those only from the d atomic orbitals (blue bars) of the Ag_{18} circle chain at the peaks X_1, X_6, Z_1 and Z_2 . Bottom: induced electron densities of the Ag_{18} circle and linear chains at the peaks X_1 (L_1), X_6 (L_3), Z_1 (T_1) and Z_2 (T_2), in which the names in the parentheses are those of the linear chain.

in the Ag_{18} linear chain. The induced electron density at the space point $\boldsymbol{r}$ is calculated according to

$$\rho_{\text{induced}}(\boldsymbol{r},\omega) = \text{Tr}\left[(\mathbf{D}(\omega) - \mathbf{D}_0)\,\Omega(\boldsymbol{r})\right], \tag{8}$$

where ω is the excitation frequency of the peak, and $\Omega_{\mu\nu}(\boldsymbol{r}) = \chi^*_\mu(\boldsymbol{r})\chi_\nu(\boldsymbol{r})$ is the overlap distribution between the atomic orbitals. The induced electron densities were calculated using the GEN1INT library,[29] and were visualized by the ParaView program[30] with a step size $0.02 \times \max(|\rho_{\text{induced}}|)$. Values close to zero, as defined by the threshold $0.1 \times \max(|\rho_{\text{induced}}|)$ was also used in order to avoid clutter in the figures, unless stated otherwise. From these induced electron densities, similar patterns are observed for the circle and linear chains for each peak, explaining the similarities of the dipole responses of these two different metallic chains.

However, being a closed curve of high symmetry, the circle chains do possess some different characteristics of the electronic excitations than the linear chains. This is clearly demonstrated by the induced electron densities in the transverse mode (peaks Z_1 and Z_2), for which the induced electron densities of the circle chains are more symmetric along the circumference, whereas differences between the end and central parts of the linear chains can easily be seen for the different electronic excitations. In contrast, the induced electron densities of the circle chains in the parallel mode, such as the peaks X_1 and X_6, can be divided into two identical parts along its diameter, as shown by the red dashed line in Fig. 3, the induced electron density in each part showing a similar pattern as that of the corresponding peak in the linear chain. The stronger spatial confinement in the circle chains explains why the energy of the peak X_1 in the Ag_{2n} circle chain is higher than that of the corresponding linear chain. It is therefore interesting to compare the dipole responses of the Ag_{2n} circle chain with that of the Ag_{n+1} linear chain. As shown in Fig. 2(a) and (b), the dipole responses of the Ag_{12} linear chain is only slightly larger than the Ag_{22} circle chain.

To briefly summarize: Bending a linear chain into a circle does not introduce new resonances in the absorption spectrum, but makes the first few peaks, for instance, X_1, Z_1 and

Z_2 blue shifted in the circle chains, demonstrating the shape dependence of the electronic excitations in these metallic chains.

3.2 Arc Chains

As for the circle and linear metallic chains, the number of atoms is an important parameter in the dipole responses of the arc chains. The calculated dipole responses of the Ag_{2n} ($n = 2, \cdots, 8$) arc and Ag_{18} circle (topmost) chains when exposed to an external δ-pulse and polarized along x (left), y (middle) and z (right) directions are shown in the top panel of Fig. 4. The radii of these arc chains are chosen to be those of the Ag_{18} circle chain, $R \approx 8.32$ Å. In Figure 4, the dipole responses of the Ag_{16} arc chain are exposed to the same δ-pulse but with the scaling parameter $\lambda = 0$ has also been shown by the red dashed lines. As is the case for the circle chains, the excitation energies obtained with $\lambda = 0$ are generally lower than those with the full two-electron contribution ($\lambda = 1$). In particular, the peaks X_1, X_1', X_6, Y_1, Y_6, Z_1 and Z_2 show a much stronger dependence on the change of the λ parameter, suggesting that these may be considered plasmon resonances.

From the spectra in Fig. 4, it is clear that the dipole responses of the arc chains in the y and z directions converge as the Ag_{18} circle chain with increasing number of atoms. However, this is not the case in the x direction — even the dipole response of the Ag_{16} arc chain shows apparent differences from that of the Ag_{18} circle chain. In particular, the first peak X_1 is blue shifted from the Ag_{16} arc chain to the Ag_{18} circle chain by adding only two more atoms. In order to rationalize this observation, we plot in the lower panel of Fig. 4 the induced electron densities of the peaks X_1 and X_1' of the Ag_{16} arc chain in three-dimensional space as well as those in the xy plane. In the latter case, only the densities with the absolute value not less than $0.5 \times \max(|\rho_{\text{induced}}|)$ are shown. The induced electron densities of the peaks X_1 and X_1' of the Ag_{16} arc chain are more similar to those of the linear chains than the circle chains — we can clearly distinguish the central and end parts of the electronic excitations in the arc chains. As such, there seems to be no reason for the dipole responses of these arc

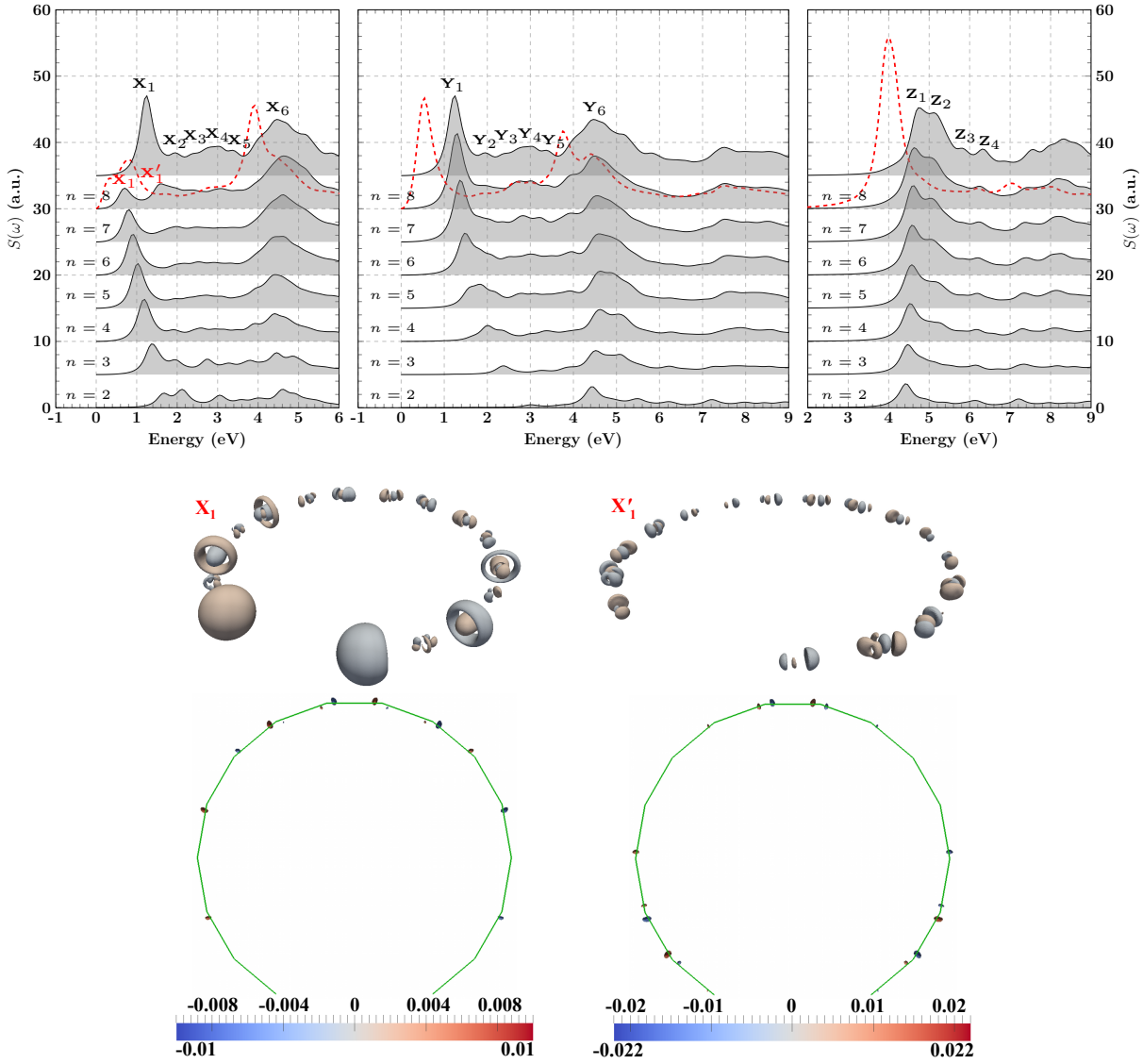

Figure 4: Top: the dipole responses of Ag_{2n} ($n = 2, \cdots, 8$) arc and Ag_{18} circle (top) chains to an external δ-pulse with strength 0.05 eV/bohr and polarized along x (left), y (middle) and z (right) directions. The red dashed lines are the dipole responses of the Ag_{16} arc chain to the same δ-pulse but with the scaling parameter $\lambda = 0$. Bottom: the induced electron densities of the peaks X_1 and X_1' of Ag_{16} arc chain in three-dimensional space as well as those on the xy plane, and in the latter, only the densities with the absolute value not less than $0.5 \times \max(|\rho_{\text{induced}}|)$ are shown.

chains along the x direction to resemble those of the Ag_{18} circle chain.

From the induced electron densities in the xy plane, we also notice the different characteristics of the peaks X_1 and X_1'. X_1 involves mainly excitations in the central part of the chain, as is the case for the first longitudinal peak in the linear chains.[18] The peak X_1', however, involves excitations on a few atoms in the central part of the chain as well as excitations in a few atoms close to the edges of the chain. As will be shown later, the different characteristics of the peaks X_1 and X_1' affect their behaviour when the chain gradually changes from a circle to a linear structure.

Another important factor that affects the excitations of the arc chain is its radius R (or equivalently its curvature $1/R$). In Fig. 5, we give the dipole responses of the Ag_{18} arc, circle and linear chains to an external δ-pulse polarized along x (left), y (middle) and z (right) directions. From bottom to top are the dipole responses of the circle ($R \approx 8.32$ Å), arc ($R = 8.5, 8.6, 8.7, 8.8, 8.9, 9, 10, 12, 15, 20, 25, 30, 40, 50, 60$ Å) and linear ($R = \infty$ Å) chains, respectively. The most striking changes in the dipole responses of these arc chains with increasing radius are (i) the split of the peak X_1 around $R = 8.6$ Å, in which the first split peak (still named as X_1) becomes stronger while the second peak X_1' gradually disappears, (ii) the disappearance and reformation of the peak X_2, (iii) the disappearance of the peaks Y_1 and Y_2, and (iv) the change of the peak Y_3 from an almost parallel mode in the arc chains (see the layout of the arc chain in Fig. 1) to the transverse mode in the linear chain. In contrast, the dipole response to the δ-pulse polarized along the z direction is almost unaffected by the change of the radius in these arc chains.

In Figure 5, we have also shown the dipole responses with scaling parameter $\lambda = 0$, of the arc chains with radius $R = 10$, 60 Å and the linear chain. The peaks X_1, Y_1, Y_3, Z_1 and Z_2 show a clear dependence on the λ parameter, suggesting that they may be considered plasmon resonances. X_3 has very different profiles between $\lambda = 0$ and $\lambda = 1$ for the arc chain with $R = 10$ Å. In the case of the arc chain with $R = 60$ Å and the linear chain, calculations give almost identical profiles with $\lambda = 0$ and $\lambda = 1$. Also shown in Fig. 6(a),

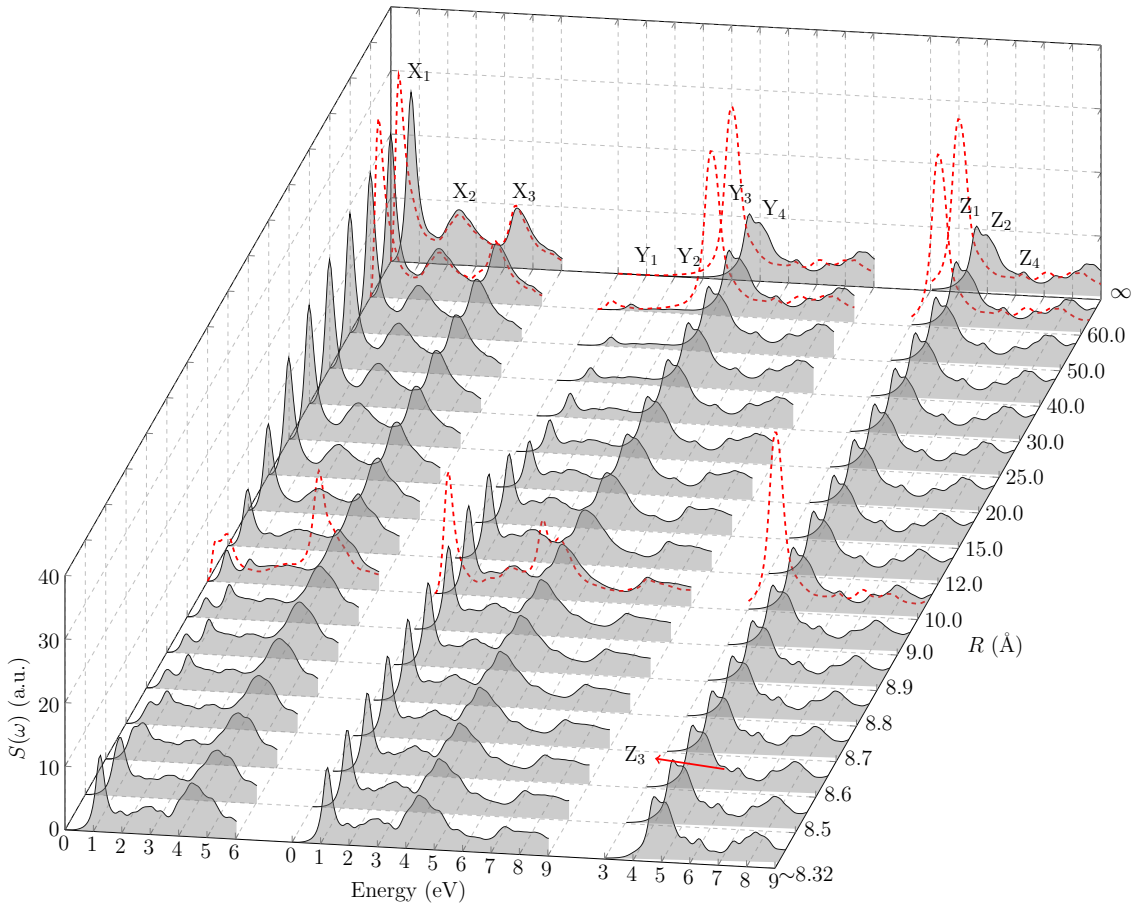

Figure 5: The dipole response of Ag_{18} arc, circle and linear chains to an external δ-pulse with strength 0.05 eV/bohr and polarized along x (left), y (middle) and z (right) directions. From bottom to top are the dipole responses of the circle chain ($R \approx 8.32$ Å), different arc chains and the linear chain ($R = \infty$ Å), in which the red dashed lines are the dipole responses of the arc chains with $R = 10$, 60 Å and the linear chain to the same δ-pulse but with the scaling parameter $\lambda = 0$.

the energy difference of the peak X_3 between $\lambda = 0$ (green triangles) and $\lambda = 1$ (blue diamonds) becomes smaller and smaller when the chain changes from the circle to the linear structure. In a study of linear gold chains, Piccini *et al.* have observed similar absorption spectra from TDDFT calculations and molecular orbital transitions.[21] It is not clear that we can attribute the peak X_3 to single-particle excitations in the arc chain ($R = 60$ Å) and the linear chain. Instead we note that in the work by Bernadotte *et al.*[19] strong mixing of plasmon and single-particle excitations was observed in a given energy range for a linear chain of 20 gold atoms, and in this case a clear-cut classification of the excitations as either plasmon or single-particle excitations is not possible. For this reason, we conclude that the excitations around the peak X_3 in these silver chains — independently of whether they are arc, circle or linear — involve a mixing of plasmon and single-particle excitations. It is easier to distinguish these two different excitation classes in the circle and arc chains (for arcs with large curvature, for instance > 0.0375 Å^{-1} as shown in Fig. 6(a)) than the linear and arc chains with a smaller curvature.

In Fig. 6, we can see the evolution of the energy positions of the individual peaks in the circle, arc, and linear chains. Except for the peak Y_3, these excitation energies are in most cases quickly red-shifted towards the value of the linear chain. However, as shown in Fig. 5, except for the z direction, the absorption profiles of the dipole responses of the arc chains become similar to those of the linear chain only after their curvatures are close to zero. To understand this observation, we plot in Fig. 7(a) and (b), respectively, the induced electron densities of the peaks X_1, Y_1 and Y_3 of the arc chains with radius $R = 10$ and 60 Å. Let us first consider the X_1 peak in the x direction, which is split into two peaks X_1 and X_1' around $R = 8.6$ Å. The latter X_1' peak becomes stronger with increasing radius, but quickly disappears again for $R \geq 12$ Å, and its excitation energy is almost constant at 1.47 eV for arc chains with radius $8.6 < R \leq 12$ Å. In contrast, the peak X_1 is gradually red-shifted and becomes stronger with increasing radius. When we earlier discussed arc chains having the same radius $R \approx 8.32$ Å but different number of atoms, we also noted the strong peak X_1',

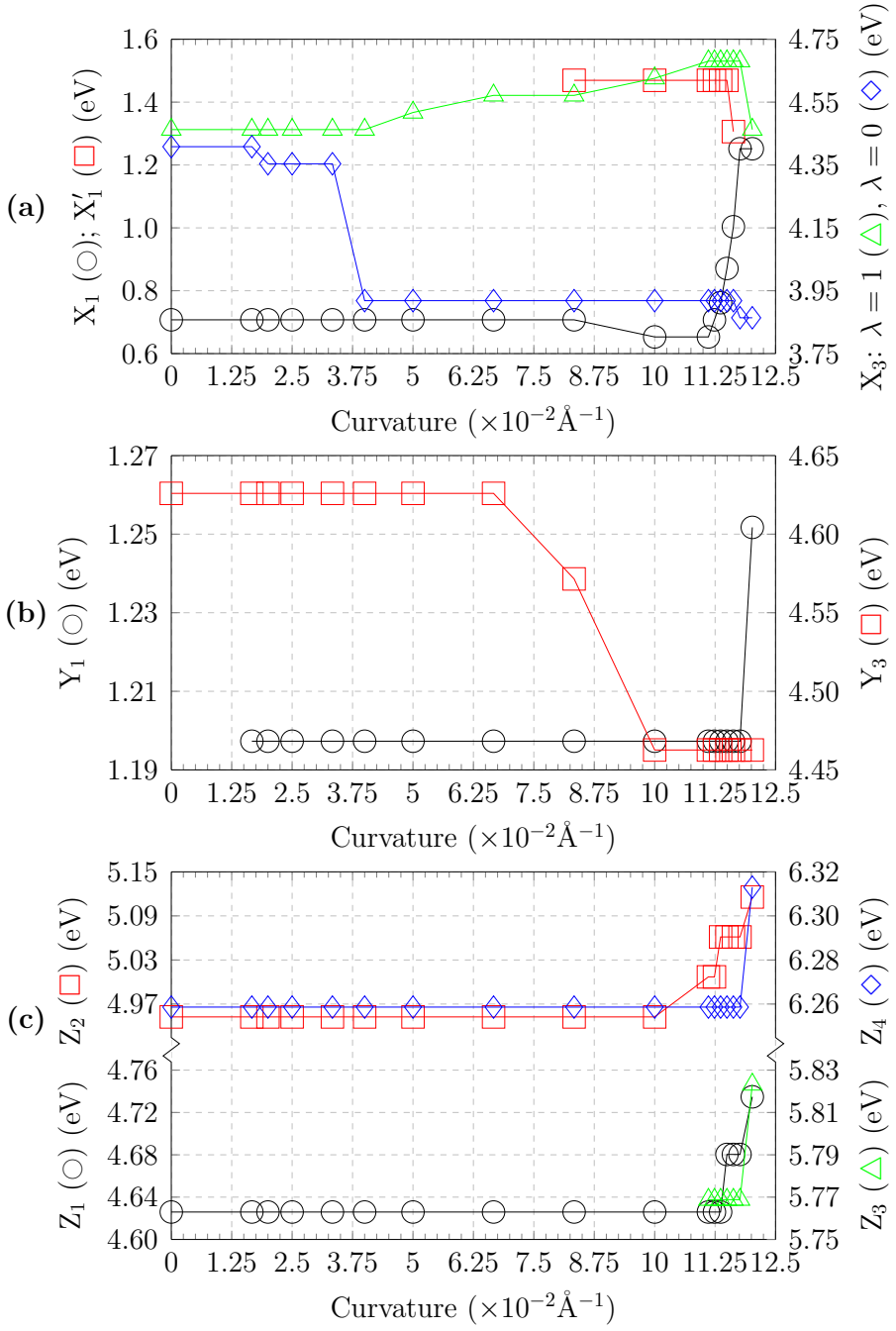

Figure 6: Energy positions of individual peaks to the δ-pulse polarized along the (a) x, (b) y and (c) z directions, respectively.

in particular in the Ag_{16} arc chain (see Fig. 4). Comparing the induced electron densities of the peaks X_1 and X_1' in these two different cases, as shown in the bottom panel of Fig. 4 (Ag_{16} arc chain with $R \approx 8.32$ Å) and Fig. 7(a) (Ag_{18} arc chain with $R = 10$ Å), one can immediately notice their similarities — the peak X_1 mostly involves excitations in the central part of the chain, whereas X_1' involves excitations happening in a few atoms in the central part and a few atoms close to the edges of the chain. As such, the peak X_1 is more sensitive to the length and geometry of the chain, showing quantum confinement effects with red-shifted excitation energies when increasing the radius of the arc chain. It also becomes much stronger when the arc chain becomes more "linear" since there will be more atoms in the central part involved in the excitations. This is illustrated by the maximum absolute values of the induced electron densities in the arc chains with $R = 10$ and 60 Å (Fig. 7(a) and (b)), 0.012 and 0.026 respectively — the latter more than twice as large as the former.

Due to the characteristic of its electronic excitations, the peak X_1' does not show a strong dependence on the radius of the arc chain, making its excitation energy almost constant and its dipole strength only slowly increase with increasing radius, until it finally is covered by the rapidly increasing strength of the X_1 peak.

The disappearance of peaks Y_1 and Y_2 can also be understood from their induced electron densities. Taking Y_1 as an example, its induced electron densities (see Fig. 7(a) and (b)) are signficantly reduced when the radius is changed from 10 Å to 60 Å. We also notice the involvement of $d \to p$ transitions in the Y_1 peak as seen from the fluctuations of the occupation numbers of the MOs in Fig. 7(c), also being reduced as the arc chain becomes more "linear", eventually being hidden in the transverse mode of the linear chain. In contrast, the intensity of the Y_3 peak does not vary a lot, but its profile changes gradually to that of the Z_1 peak (T_1) in the linear chain. This can also be seen from its induced electron densities: compared to the induced electron densities of the arc chain with radius $R = 10$ Å, the induced electron density of the arc chain with $R = 60$ Å resemble to a much greater extent that of the T_1 peak in the linear chain (see Fig. 3).

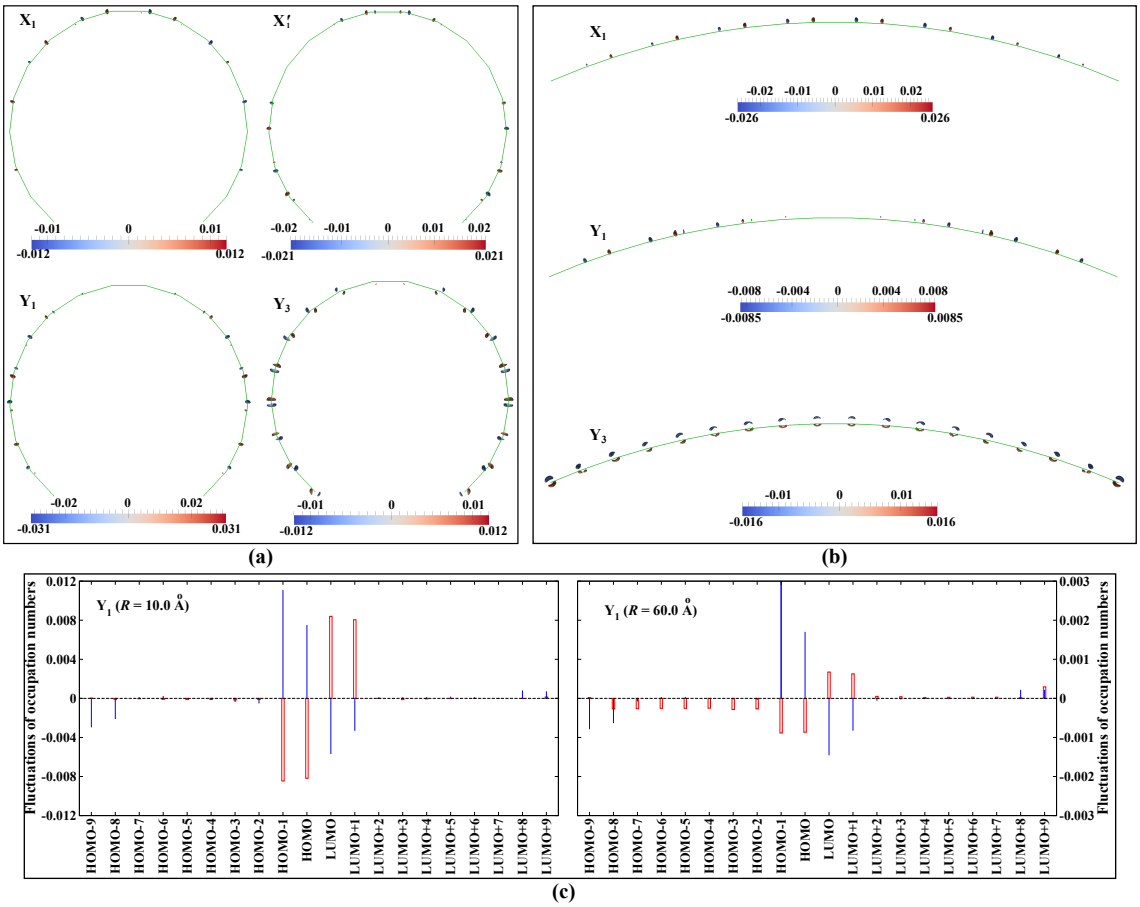

Figure 7: (a): the induced electron densities on the xy plane of peaks X_1 and X_1', and the induced electron densities of peaks Y_1 and Y_3 of the Ag_{18} arc chain with radius $R = 10$ Å. (b): the induced electron densities of peaks X_1, Y_1 and Y_3 of the Ag_{18} arc chain with radius $R = 60$ Å. In (a) and (b), only the densities with the absolute value not less than $0.5 \times \max(|\rho_{\text{induced}}|)$ are shown. (c): the fluctuations of the occupation numbers of the MOs (total: red open bars, d orbitals: blue bars) of peak Y_1 of the Ag_{18} arc chains with the radius $R = 10$ and 60 Å.

Summarizing our findings for the arc chains, we recall that both the size (number of atoms) and geometric structure (radius or curvature) of the arc chains are important for their electronic excitations. This allows interesting energy ranges for photon absorption to be accessed either by altering the size or the shape of the metallic chains.

3.3 Zigzag Chains

Finally we will consider zig-zag chains, still taking the 18 silver atom chain as an example to demonstrate the shape dependence of the electronic excitations in these chains. The dipole responses to an external δ-pulse of different Ag_{18} zigzag chains and the linear chain are shown in Fig. 8(a), in which the δ-pulse is polarized along x, y and z directions from left to right, and from bottom to top in each panel are the dipole responses of the linear ($\theta = 180°$) and different zigzag chains with bond angle θ as $170°, 160°, \cdots, 60°$, respectively.

In contrast to the circle and arc chains, the dipole responses of the zigzag chains show obvious differences compared to the linear chain, not only in the x and y directions but also in the z direction. In particular, there are new peaks arising in the y (peak Y_1) and z (peak Z_1) directions in the zigzag chains, which together with peaks X_1, Y_2 and Z_2 are more sensitive to the scaling parameter λ — as can be seen by comparison to the dipole responses from calculations with $\lambda = 0$, the red dashed lines in Fig. 8(a). The peak X_3 may involve, as discussed in the previous section, the mixing of plasmon and single-particle transitions so that the spectra from calculations with $\lambda = 0$ and $\lambda = 1$ resemble each other around the X_3 peak.

As shown in Fig. 8(b), most peaks become blue shifted when the bond angle θ decreases from 180° (linear chain) to 60°, except for peaks X_3 and Y_2. The former is almost constant at about 4.5 eV and involves $d \rightarrow p$ transitions (from its fluctuations of the occupation numbers of the MOs, not shown here), very similar to the peak L_3 in the linear chain, and X_6 and X_3 in the circle and arc chains. The Y_2 peak instead shows a red shift with decreasing bond angle θ, opposite of what is observed for Y_1. The different behaviours of peaks Y_1 and

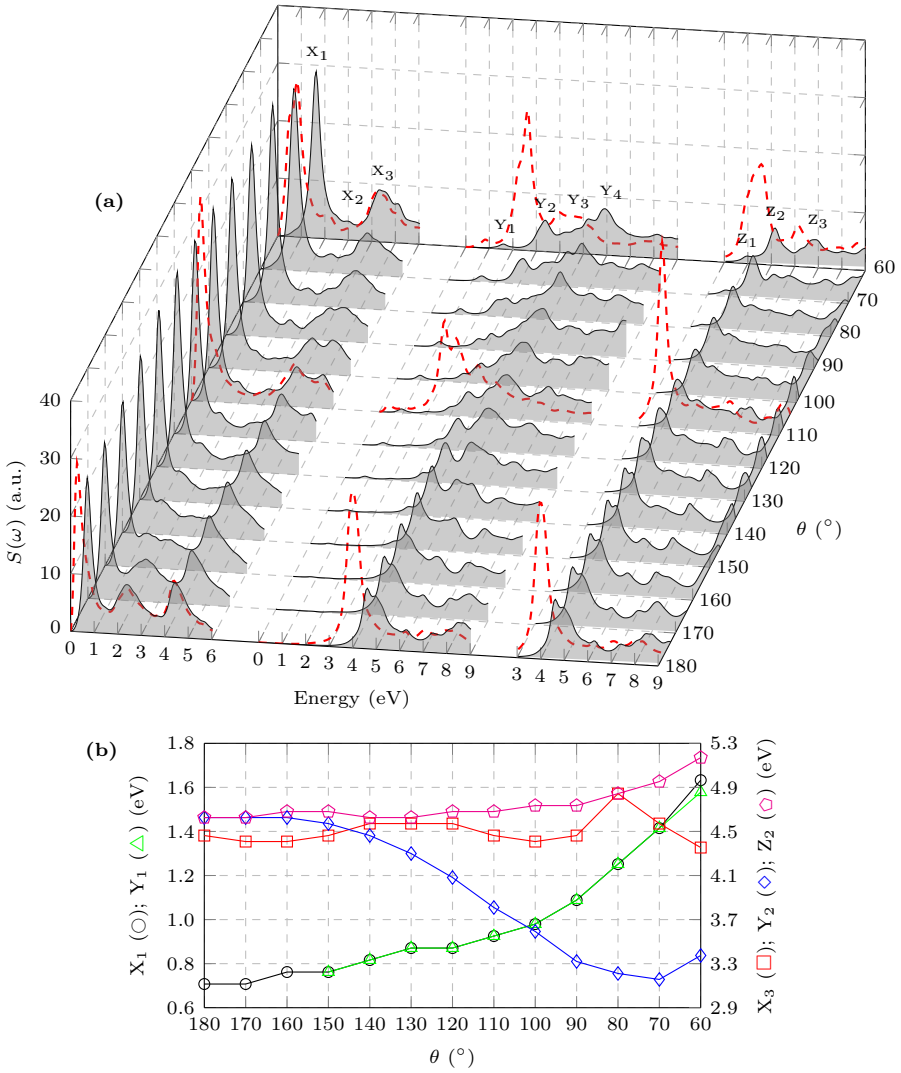

Figure 8: (a): dipole responses of different Ag_{18} zigzag chains and the linear chain to an external δ-pulse with strength 0.05 eV/bohr and polarized along x (left), y (middle) and z (right) directions. From bottom to top are respectively the dipole responses of the linear ($\theta = 180°$) and zigzag ($\theta = 170°, 160°, \cdots, 60°$) chains, in which the red dashed lines are the dipole responses of the linear chain and zigzag chains with $\theta = 110°$ and $60°$ to the same δ-pulse but with the scaling parameter $\lambda = 0$. (b): energy positions of individual peaks to the δ-pulse with respect to the bond angle θ.

Y_2 can be qualitatively understood from their different induced electron densities shown in Fig. 9. In particular, the electronic excitations in the Y_1 peak are mostly localized on the ends of the chain, whereas the Y_2 peak shows a clearly delocalized picture.

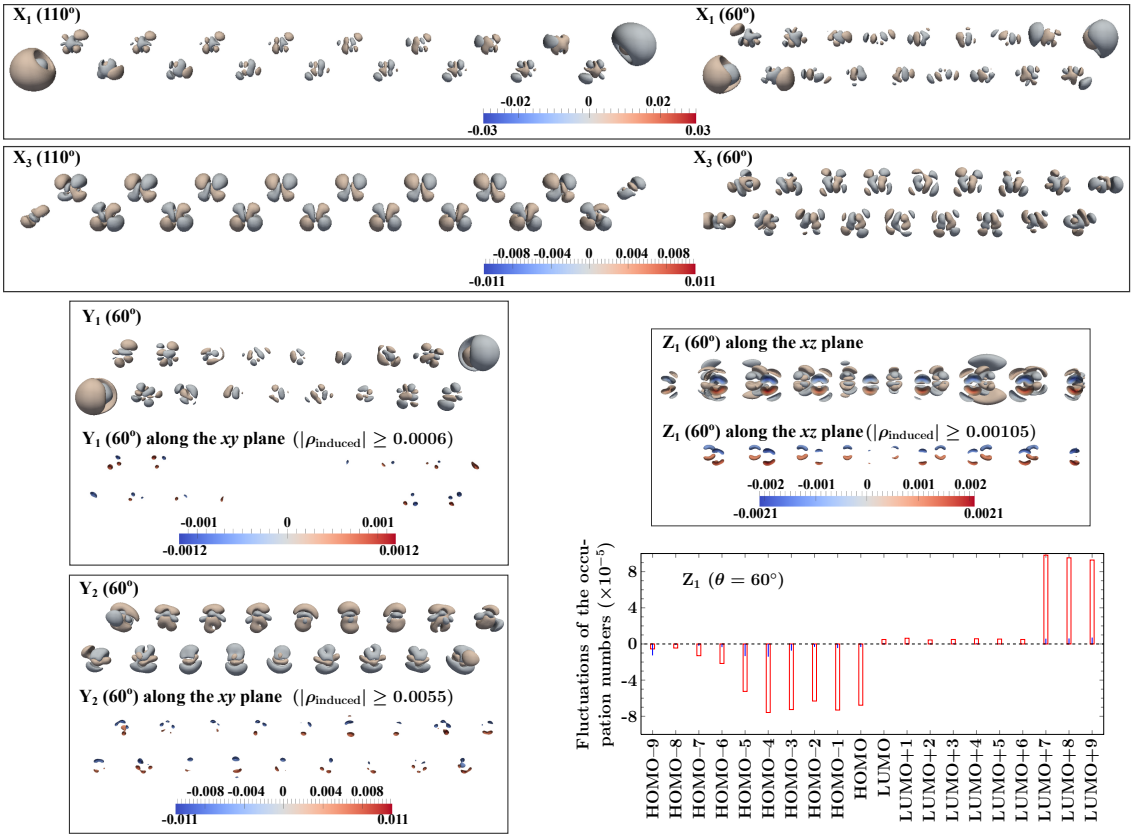

Figure 9: From top to bottom: the induced electron densities of the peaks X_1 and X_3 of the Ag_{18} zigzag chain with bond angle $\theta = 110°$, the induced electron densities of the peaks X_1, X_3, Y_1 and Y_2 of the Ag_{18} zigzag chain with $\theta = 60°$, and the induced electron densities on the xy plane of the peaks Y_1 and Y_2 and that on the xz plane of the peak Z_1 of the Ag_{18} zigzag chain with $\theta = 60°$. The fluctuations of the occupation numbers of the MOs (total: red open bars, d orbitals: blue bars) of the peak Z_1 in the Ag_{18} zigzag chain with $\theta = 60°$ are also shown at the bottom right corner.

From a consideration of the induced electron densities of the peaks X_1 and X_3, for example, one can also view the zigzag chains as double linear chains with the two end parts localized on different chains. Therefore, one may imagine that decreasing the bond angle θ corresponds to the decrease of length of the double linear chains and the decrease of internuclear distance in each of the double linear chains, both of which will result in a blue shift of the excitation energies of some peaks.

Finally, we note the appearance of the new peak Z_1 in the z direction (the transverse mode), whose excitations also involve the d electrons as shown from the fluctuations of the occupation numbers of the MOs in Fig. 9. Moreover, from its induced electron density shown in Fig. 9, we can clearly observe the collective excitation picture. As such, the zigzag chains provide us a new peak with collective excitations in transverse mode but with even lower excitation energy comparing with the linear, circle and arc chains. This also suggests that interesting optical properties may be found in, for instance metallic planes,[31] multiple layers of a metal sheet or thin-films of metal atoms.

4 CONCLUSIONS

We have shown that great flexbility in tuning of electronic excitations in metallic chains is possible by altering their geometric structures. Different structures of silver chains — circle, arc and zigzag chains — have been investigated at the TDDFT level, demonstrating the tunability of their electronic excitations by simply altering their geometric parameters: the radius of the circle and arc chains, and the bond angle of the zigzag chains.

New dipole responses have arisen in the arc and zigzag chains. Some of these even have as wide a tunable excitation energy range as 1 eV, as shown in Fig. 6(a) and Fig. 8(b). In particular, the zigzag chains have shown fine-tunable optical properties as illustrated in Fig. 8(b) — the excitation energies of individual peaks change smoothly as a function of the bond angle. All these unique properties make it possible to control the excitations of these chains at an atomic scale — for instance by manipulating atoms with the scanning tunneling microscope.

The study of the zigzag chains also suggests that future work could be carried out on two-dimensional metallic planes, multiple layers of a metal sheet or thin-films of metal atoms, just name a few. New and interesting optical properties may be found in these low-dimensional metallic systems.

Acknowledgement

This work has received support from the Research Council of Norway through a Centre of Excellence grant (Grant No 179568/V30) and a European Research Council (ERC) Starting Grant (Grant No 279619). This work has also received support from the Norwegian Supercomputing Program (NOTUR) through a grant of computer time (Grant No. NN4654K).

References

(1) Springborg, M.; Dong, Y. Elemental Chains. *Int. J. Quantum Chem.* **2009**, *109*, 837–848.

(2) Bahn, S. R.; Jacobsen, K. W. Chain Formation of Metal Atoms. *Phys. Rev. Lett.* **2001**, *87*, 266101.

(3) Amorim, E. P. M.; da Silva, E. Z. *Ab Initio* Study of Linear Atomic Chains in Copper Nanowires. *Phys. Rev. B* **2010**, *81*, 115463.

(4) Amorim, E. P. M.; da Silva, A. J. R.; Fazzio, A.; da Silva, E. Z. Short Linear Atomic Chains in Copper Nanowires. *Nanotechnology* **2007**, *18*, 145701.

(5) Fioravante, F.; Nunes, R. W. Semiconducting Chains of Gold and Silver. *Appl. Phys. Lett.* **2007**, *91*, 223115.

(6) Springborg, M.; Sarkar, P. Structural and Electronic Properties of Thin Chains of Ag. *Phys. Rev. B* **2003**, *68*, 045430.

(7) Sánchez-Portal, D.; Artacho, E.; Junquera, J.; Ordejón, P.; García, A.; Soler, J. M. Stiff Monatomic Gold Wires with a Spinning Zigzag Geometry. *Phys. Rev. Lett.* **1999**, *83*, 3884–3887.

(8) Ribeiro, F. J.; Cohen, M. L. Ab Initio Pseudopotential Calculations of Infinite Monatomic Chains of Au, Al, Ag, Pd, Rh, and Ru. *Phys. Rev. B* **2003**, *68*, 035423.

(9) Calzolari, A.; Buongiorno Nardelli, M. First Principles Theory of Artificial Metal Chains on NiAl(110) Surface. *Phys. Rev. B* **2005**, *72*, 045416.

(10) Skorodumova, N. V.; Simak, S. I.; Kochetov, A. E.; Johansson, B. Length Dependence of the Electronic and Structural Properties of Monoatomic Gold Wires. *Phys. Rev. B* **2005**, *72*, 193413.

(11) Nilius, N.; Wallis, T. M.; Ho, W. Development of One-Dimensional Band Structure in Artificial Gold Chains. *Science* **2002**, *297*, 1853–1856.

(12) Yan, J.; Yuan, Z.; Gao, S. End and Central Plasmon Resonances in Linear Atomic Chains. *Phys. Rev. Lett.* **2007**, *98*, 216602.

(13) Yan, J.; Gao, S. Plasmon Resonances in Linear Atomic Chains: Free-Electron Behavior and Anisotropic Screening of *d* Electrons. *Phys. Rev. B* **2008**, *78*, 235413.

(14) Lian, K.-Y.; Sałek, P.; Jin, M.; Ding, D. Density-Functional Studies of Plasmons in Small Metal Clusters. *J. Chem. Phys.* **2009**, *130*, 174701.

(15) Chen, C.; Bobisch, C. A.; Ho, W. Visualization of Fermi's Golden Rule Through Imaging of Light Emission from Atomic Silver Chains. *Science* **2009**, *325*, 981–985.

(16) Morton, S. M.; Silverstein, D. W.; Jensen, L. Theoretical Studies of Plasmonics using Electronic Structure Methods. *Chem. Rev.* **2011**, *111*, 3962–3994.

(17) Gao, B. TDRsp Version 0.2.0. 2012; `http://repo.ctcc.no/projects/tdrsp`, TDRsp is a tool package solving the equation of motion of reduced single-electron density matrix in the framework of Hartree-Fock or density functional theory in time domain, and will be released under the GNU Lesser General Public License.

(18) Gao, B.; Ruud, K.; Luo, Y. Plasmon Resonances in Linear Noble-Metal Chains. *J. Chem. Phys.* **2012**, *137*, 194307.

(19) Bernadotte, S.; Evers, F.; Jacob, C. R. Plasmons in Molecules. *J. Phys. Chem. C* **2013**, *117*, 1863–1878.

(20) Bernadotte, S. Plasmons in Nanostructures with Applications to Metamaterial Science. Ph.D. thesis, Karlsruher Institut für Technologie (KIT), 2011.

(21) Piccini, G.; Havenith, R. W. A.; Broer, R.; Stener, M. Gold Nanowires: A Time-Dependent Density Functional Assessment of Plasmonic Behavior. *J. Phys. Chem. C* **2013**, *117*, 17196–17204.

(22) Baishya, K.; Idrobo, J. C.; Öğüt, S.; Yang, M.; Jackson, K. A.; Jellinek, J. First-Principles Absorption Spectra of Cu_n ($n = 2 - 20$) Clusters. *Phys. Rev. B* **2011**, *83*, 245402.

(23) Nazin, G. V.; Qiu, X. H.; Ho, W. Atomic Engineering of Photon Emission with a Scanning Tunneling Microscope. *Phys. Rev. Lett.* **2003**, *90*, 216110.

(24) Lopata, K.; Govind, N. Modeling Fast Electron Dynamics with Real-Time Time-Dependent Density Functional Theory: Application to Small Molecules and Chromophores. *J. Chem. Theory Comput.* **2011**, *7*, 1344–1355.

(25) Dalton. 2005; `http://www.kjemi.uio.no/software/dalton/dalton.html`, a molecular electronic structure program, Release 2.0 (2005).

(26) Perdew, J. P.; Chevary, J. A.; Vosko, S. H.; Jackson, K. A.; Pederson, M. R.; Singh, D. J.; Fiolhais, C. Atoms, Molecules, Solids, and Surfaces: Applications of the Generalized Gradient Approximation for Exchange and Correlation. *Phys. Rev. B* **1992**, *46*, 6671–6687.

(27) Andrae, D.; Häußermann, U.; Dolg, M.; Stoll, H.; Preuß, H. Energy-Adjusted *Ab Initio* Pseudopotentials for the Second and Third Row Transition Elements. *Theor. Chim. Acta* **1990**, *77*, 123–141.

(28) Lopata, K.; Govind, N. Modeling Fast Electron Dynamics with Real-Time Time-Dependent Density Functional Theory: Application to Small Molecules and Chromophores. *J. Chem. Theory Comput.* **2011**, *7*, 1344–1355.

(29) Gao, B.; Thorvaldsen, A. J. Gen1Int Version 0.2.1. 2012; `http://repo.ctcc.no/projects/gen1int`, Gen1Int is a library to evaluate the derivatives of one-electron integrals with respect to the geometry perturbation, external electric and magnetic fields, and total rotational angular momentum at zero fields with contracted rotational London atomic orbitals (LAO), and is released under the GNU Lesser General Public License.

(30) Henderson, A. *ParaView Guide: A Parallel Visualization Application*; Kitware Inc.: New York, 2007.

(31) Wang, B.-J.; Xu, Y.; Ke, S.-H. Plasmon Excitations in Sodium Atomic Planes: A Time-Dependent Density Functional Theory Study. *J. Chem. Phys.* **2012**, *137*, 054101.

Graphical TOC Entry